A&A 514, A68 (2010)
DOI: 10.1051/0004-6361/200913477

Astronomy & Astrophysics

Velocity vectors of a quiescent prominence observed by *Hinode*/SOT and the MSDP (Meudon)⋆

B. Schmieder[1], R. Chandra[1], A. Berlicki[2], and P. Mein[1]

[1] Observatoire de Paris, LESIA, UMR8109 (CNRS), 92195 Meudon Principal Cedex, France
e-mail: brigitte.schmieder@obspm.fr
[2] Astronomical Institute, Academy of Sciences, Ondřejov, Czech Republic

Received 15 October 2009 / Accepted 13 January 2010

ABSTRACT

Context. The dynamics of prominence fine structures present a challenge to our understanding of the formation of cool plasma prominence embedded in the hot corona.
Aims. Observations performed by the high resolution *Hinode*/SOT telescope allow us to compute velocities perpendicular to the line-of-sight or transverse velocities. Combining simultaneous observations obtained in Hα with *Hinode*/SOT and the MSDP spectrograph operating in the Meudon solar tower, we derive the velocity vectors of a quiescent prominence.
Methods. The velocities perpendicular to the line-of-sight are measured using a time-slice technique and the Doppler shifts velocity using the bisector method.
Results. The Doppler shifts of bright threads derived from the MSDP show counterstreaming of the order of 5 km s^{-1} in the prominence and reaching 15 km s^{-1} at the edges of the prominence. Even though they are minimum values because of seeing effects, they are of the same order as the transverse velocities.
Conclusions. These measurements are very important because they suggest that the vertical structures detected by SOT may not be true vertical magnetic structures in the sky plane. The vertical structures could be a pile up of dips in more or less horizontal magnetic field lines in a 3D perspective, as proposed by many MHD modelers. In our analysis, we also calibrate the *Hinode* Hα data using MSDP observations obtained simultaneously.

Key words. Sun: filaments, prominences – magnetic fields

1. Introduction

The existence of cool structures in so-called prominences and filaments over a few solar rotations embedded in the hot corona has been a mystery since the beginning of their spectrographic observations (d'Azambuja & d'Azambuja 1948). Many reviews describe the study of quiescent prominences (Schmieder 1989; Tandberg-Hanssen 1994; Labrosse et al. 2010; Mackay et al. 2010). It has been a challenge to ascertain the most effective mechanism for maintaining cool plasma in the corona. A very popular idea is that the plasma is frozen in magnetic field lines and it kept cool by the low transverse thermal conduction (Démoulin et al. 1989). Many magnetic and static models have been developed based on this idea (Kuperus & Raadu 1974; Kippenhahn & Schlüter 1957; Aulanier & Démoulin 1998a; Dudík et al. 2008). However, a significant question remains: how can the cool plasma inside the field lines be transported into the corona and kept there? It is recognized that this material should come from the chromosphere by either levitation or injection (Saito & Tandberg-Hanssen 1973). Sufficient mass must be extracted from the chromosphere by either magnetic forces that inject or lift the plasma or pressure forces that evaporate the plasma and then cool it to prominence temperatures. Many models have been developed in this sense, i.e., thermal non-equilibrium models (Mariska & Poland 1985; Karpen et al. 2003, 2005). Levitation models are proposed that are based on possible magnetic reconnection (van Ballegooijen & Martens 1989). Injection models can incorporate injection by means of the reconnection of magnetic field during canceling flux. These models indicate that the plasma in prominences should have significant dynamical motion and static models may be obsolete. Observations performed by the Swedish Solar Telescope (SST) show highly dynamic plasma in filament threads (Lin et al. 2003, 2005) and were also used in a first attempt to compute the velocity vectors of the filament threads. The authors conclude that the threads' inclinations from the horizontal were about 16 degrees with a net flow in both directions of 8 km s^{-1}. Fine counterstreaming flow is often observed either along horizontal threads or in the barbs (Zirker et al. 1998; Schmieder et al. 1991, 2008). *Hinode*/SOT movies (available with the electronic version of the paper) illustrate the significant dynamics of the prominence fine structures. The spicules close to the barbs could allow us to inject plasma inside the fine threads. Is this sufficient to continuously feed the main core of the prominence? A mass budget should be performed. Using *Hinode* observations at the limb, Berger et al. (2008) and Chae et al. (2008) attemped to answer these questions. They reported different velocity measurements. Berger et al. (2008) found upward motions of dark bubbles around 20 km s^{-1} and downward flows of bright knots moving more slowly than 10 km s^{-1} by analysing Ca II H images at the line center. Chae et al. (2008) analyzed a hedgerow prominence and found horizontal displacements before observing downflows of bright knots, which are all indicative of vortex motions.

⋆ A movie is available in electronic form at http://www.aanda.org

Prominence dynamics at the limb appear to differ significantly from filament dynamics on the disk. The integration along the line of sight complicates the interpretation. **?** show that more than 15 threads may be integrated along the line of sight and the resulting velocities should depend on two different Gaussian distributions. At the edges of prominences, the velocity values are higher because fewer threads are integrated and velocity cells are larger than intensity knots, which implies that bunches of threads may move with the same velocity plasma (Doppler shifts). Similar results were found by adopting completely different approaches. To reproduce Lyman line profiles observed by SOHO/SUMER, Gunár et al. (2007) therefore introduce 10 threads perpendicular to the line-of-sight with a random velocity distribution in a 2D non-LTE radiative transfer code.

In this study we propose to study both the velocity perpendicular to the line of sight using one hour of observations of *Hinode*/SOT in Hα combined with Doppler shifts observed also in Hα with the Multichannel Subtractive Double Pass spectrograph (MSDP) operating in the Meudon solar tower. These observations were obtained simultaneously during a coordinated observing program (JOP178). Using *Hinode* data, it is the first time that these fine structures have been resolved in prominences and that oscillations and transverse velocities have been able to be derived (Okamoto et al. 2007; Berger et al. 2008; Chae et al. 2008). *Hinode* has a much higher spatial resolution than MSDP by a factor of 5, but the MSDP observations are very useful for calculating the Doppler shifts and calibrating the intensity of *Hinode*/SOT observations.

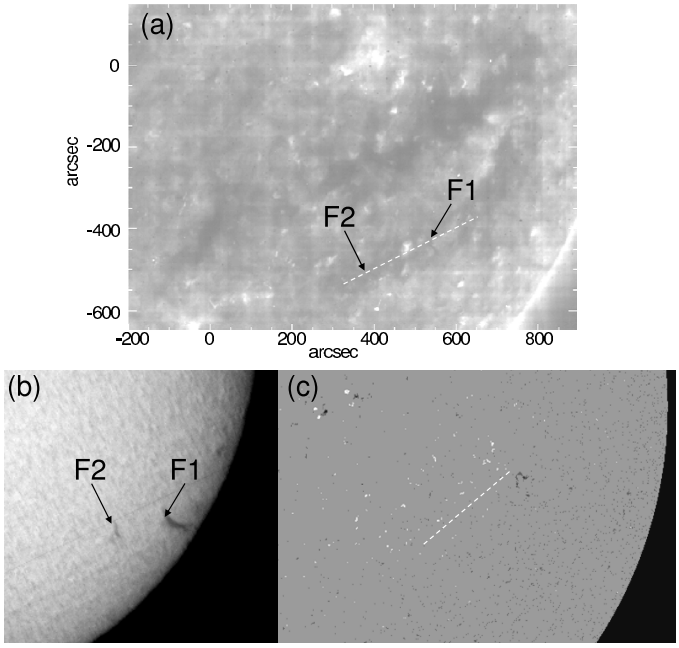

Fig. 1. a) EIT 304 Å image observed on April 20, 2007 at 01:00 UT, the field of view is 1100 × 750 arcsec, **b**) Filament observed in Hα at Meudon on April 22, 2007 at 15:28 UT, **c**) MDI longitudinal magnetic field on April 21 at 08:00 UT. The magnetic inversion line is represented by the dashed line in the middle of the EUV filament channel and in the MDI image. The letters F1 and F2 indicate approximately the location of the two filament fragments visible in Hα.

2. Observations

The observations presented here were performed during a coordinated campaign of prominence observations involving *Hinode*, SOHO, and TRACE missions, as well as several ground-based observatories. These observations were performed in the JOP 178 framework during the interval April 23–29 2007 of the first SUMER-*Hinode* observing campaign. JOP 178 (HOP 111) had been performed successfully many times in the past (see[1]). JOP 178 is dedicated to the study of prominences and filaments, investigating for example their three-dimensional structure and magnetic environment between the photosphere and the corona. The observations of the cavity of the prominence completed principally by *Hinode*/XRT and TRACE were described in detail by Török et al. (2009) and Heinzel et al. (2008). The prominence is difficult to observe on the disk. Two fragments, F1 and F2 were observed on April 21 and 22 2007 in Hα survey spectroheliograms at Meudon (Fig. 1). On April 21, they were located at S 33 W 40–50 degrees for F1 and S 35 W 35 degrees for F2. With a "Y" shape F1 has one branch aligned along a parallel and the other inclined. It crosses the limb on April 25. The angle P is negative, the leading part of F1 being further south than the following part F1 as it crosses the limb. These two fragments represent the denser parts of a filament and appear to be the feet, the main body being less dense and invisible in the survey observations as commonly found (Malherbe 1989). EIT observes a large dark filament channel on April 21 between an area of positive magnetic flux in the north and negative polarities in the south. The longitudinal magnetic flux is weaker than 10 G in absolute value. It is difficult to derive the polarity inversion line even when the filament is in the middle of the west quadrant on April 20 (Fig. 1). This prominence is extremely quiescent.

[1] http://bass2000.obs-mip.fr/jop178/index.html

2.1. Hinode/SOT observations

The *Hinode* mission has been operating since October 2006 (Kosugi et al. 2007). The prominence studied here was well observed by the *Hinode*/SOT instrument between 13:04 and 13:59 UT in both Hα and Ca II H lines on April 25, 2007. The 50 cm diameter SOT can obtain a continuous, seeing-free series of diffraction-limited images in the 388–668 nm wavelength range with 0.2–0.3 arcsec spatial resolution. The field-of-view of CaII H line is smaller (108 × 108 arcsec) and does not cover the whole prominence. In our study, we use only Hα images (160 × 160 arcsec) registered as a 1024 × 1024 pixels matrix, each pixel having dimensions of 0.16 × 0.16 arcsec. The SOT NFI filter is centered on the Hα line (determined in a line-scan calibration prior to the observations) with a bandpass width of 120 mÅ. Prominences with Doppler shifts larger than 20 km s^{-1} cannot be observed because the maximum intensity would be outside the bandpass. The center of the field-of-view in solar coordinates was [830, –510] arcsec and the exposure time 300 ms. The images were dark-subtracted and flat-fielded to remove CCD fringes in the Hα images (Fig. 2). The images were sharpened by applying an unsharp mask procedure to increase the fine structure contrast. Looking at the Hα SOT movie, we observe that the fine structures of the prominences evolve very rapidly, particularly the round-shaped structures, i.e., dark "bubbles" at the bottom of the prominence. They rise maintaining their half circle shapes. The material in the prominence lying above these dark features is very dynamic as these features rise. The material in the bright structures appears to descend. We observe from time to time brighter threads surrounding the top of the bubbles which have accelerated velocities. The dynamics of this prominence are comparable to those of the hedgerow prominence described by Berger et al. (2008).

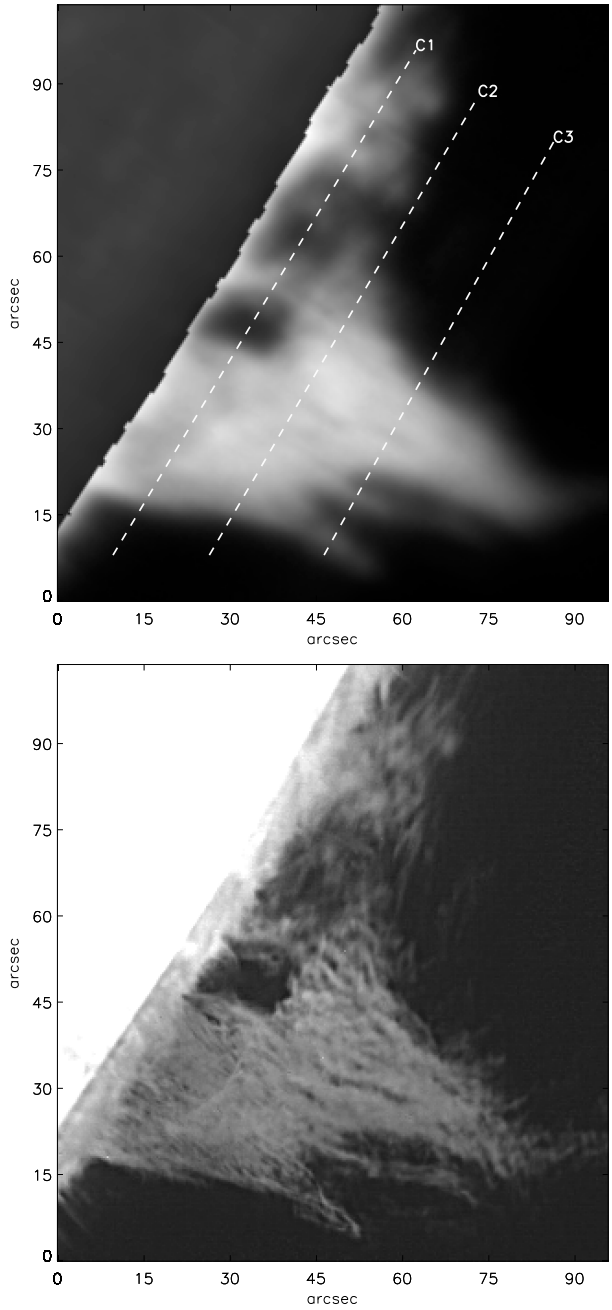

Fig. 2. *Top panel*: observation of the prominence in Hα line center by the MSDP spectrograph at 13:19:56 UT. *Bottom panel*: Hα image of prominence with *Hinode*/SOT at 13:19:50 UT on 25 April 2007. The 3 cuts used for the calibration are indicated in the top panel. A movie obtained with high cadence images of SOT, available on-line, shows the evolution of the prominence.

2.2. MSDP observations

The prominence was observed during three consecutive days, on the April 24, 25, 26 with the Multichannel Subtractive Double Pass spectrograph (MSDP) operating in the solar tower of Meudon. On April 25, the prominence was observed between 12:09 and 13:32 UT. The entrance field stop of the spectrograph covers an elementary field-of-view of 72 × 465 arcsec with a pixel size of 0.5 arcsec. The final field-of-view of the images is 500 × 465 arcsec. The exposure time is 250 ms. We performed consecutive sequences of 60 images with a cadence of 30 s. The spatial resolution is estimated to be between of 1 arcsec and 2 arcsec depending on the seeing. Using the MSDP technique (Mein 1977, 1991; Mein & Mein 1991), the Hα image of the field-of-view is devided in wavelength into nine images covering the same field of view. The nine images are recorded simultaneously on a CCD Princeton camera. Each image is obtained in a different wavelength interval. The wavelength separation between the center wavelength of one image to the next is 0.3 Å. By interpolating using spline functions between the observed intensity in these images, we are able to construct Hα profiles at each point of the observed field-of-view. A mean or reference disk profile is obtained by averaging over a quiet region of the disk in the vicinity of the prominence (this case at $\sin\theta = 0.98$). The photometric calibration is performed by fitting the reference profile to standard profiles for the quiet Sun (David 1961). We corrected the profile of the scattering light by study the nearby corona. The observations of the prominence at the Hα line center by the MSDP spectrograph are easily coaligned with the Hα SOT images obtained at the same time (Fig. 2).

2.3. Normalization of the Hα intensities

The normalization of Hα intensity allows observations to be compared with theoretical Hα profiles provided by radiative transfer codes (Gouttebroze et al. 1993; Heinzel et al. 2005) leading to the determination of physical quantities of prominences. This step is beyond the scope of this paper. Nevertheless, it is interesting to calibrate the *Hinode* data using the MSDP data. The intensities of the MSDP observed profiles are normalized to the local continuum $I_\lambda/(I_{\rm c,loc})_{\rm obs}$, and the intensities of the local continuum to the continuum at the disk center $I_{\rm (c,loc)}/(I_{\rm c})$. The continuum at disk center in the wavelength region close to the Hα line is according to David (1961)

$$I_{\rm c} = 4.077 \times 10^{-5} \text{ erg cm}^{-2} \text{ s}^{-1} \text{ sr}^{-1} \text{ Hz}^{-1}.$$

To perform the normalization, we must apply two corrections: (i) one related to the limb darkening, the reference profiles being measured on the disk near the limb at $\sin(\theta) = 0.98$. This reduces the intensity by a factor 0.547; (ii) a second that takes into account the θ angle, and the central intensity being no longer equal to 16% of the intensity of the continuum but to 22.6% of the intensity of the continuum for $\sin(\theta) = 0.98$. We present cuts drawn parallel to the limb at 3 different altitudes over the limb through the MSDP prominence (see the positions of the cuts in Fig. 2 top panel). The SOT prominence cuts at the same positions have been plotted onto the MSDP cuts (the bubbles having a contrast of between 70 to 90%, Fig. 3). The MSDP cuts are smooth with lower contrasts compared to SOT cuts because of the seeing. This allows us to calibrate the Hα SOT observations. This is valid with some possible translation depending on the accuracy of the wavelength determination. Using the count numbers of the SOT Level-1 file, we derive the calibration curve shown in Fig. 4. The integrated Hα intensity of bright threads are around 1.5×10^5 erg/s/sr/cm^2.

3. Doppler shifts

A Doppler-shift map is presented in Fig. 5. We note the trend of the velocity pattern with to have successive vertical blue- and red-shifted, elongated cells or strands. The trend of this pattern evolves slightly during an hour of observations. We compute the velocity $V(y)$, in a reference system (x, y, z), where (x, z) represents the plane of the sky. In the computation, we use the bisector method. The velocity values do not depend on the selected

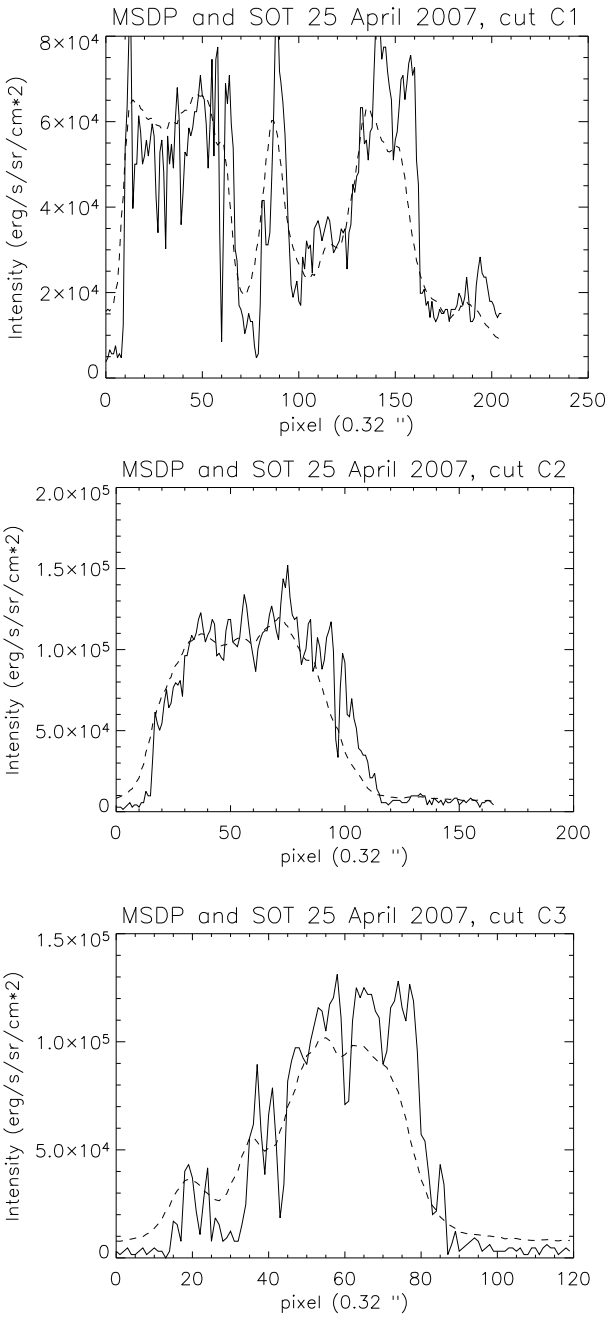

Fig. 3. Calibrated intensities of cuts (dashed lines) through the prominence parallel to the limb observed by MSDP from the south to the north overlaid by cuts (solid lines) obtained through the SOT image of the same prominence at the same time (13:19 UT) for 3 different altitudes 7.5, 18.7, and 30 Mm above the solar limb. Cut 1 is below the main prominence and crosses the bubbles. It is more extended than the other cuts. The cut locations are indicated in Fig. 2.

$\Delta(\lambda)$ of the bisector because the profiles are rather symmetric and narrow. The accuracy of the measurements is estimated by a simulation program to be less than 1 km s^{-1}. Close to the top of the prominence, we measure counterstreaming with red shifts of 15 km s^{-1} and blue shifts of –5.5 km s^{-1} (Table 1). In the central part of the prominence, the absolute velocity of each thread is between 1 to 4 km s^{-1}. At the top of the bubble, bright threads move with a velocity of 7 km s^{-1}. The location of the 12 points mentioned in Table 1 are indicated in Fig. 5. The profiles of the Hα line are all relatively narrow (Fig. 6). This means that the

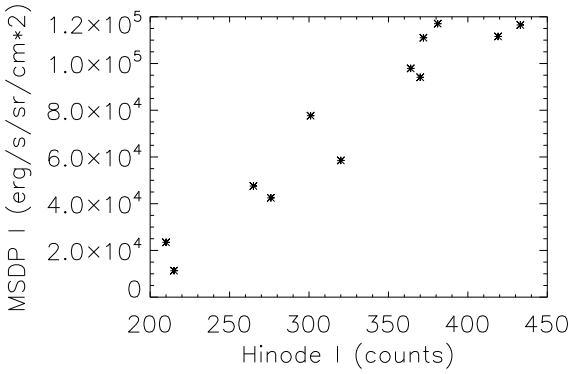

Fig. 4. Counts of the Hα SOT intensity versus calibrated MSDP integrated intensity in erg/s/sr/cm^2. The plot shows linear behavior.

different threads along the line of sight have similar velocity but are still of somewhat lower value because of smearing and seeing effects. This should also be true for threads close to each other in the same pixel. It is difficult to estimate the filling factor. Fine structures are tied in bunches. This result was also obtained for previous observations (Mein & Mein 1991; 1991).

4. Velocity perpendicular to the line-of-sight

The *Hinode* movie shows tremendous downflows of mainly the bright threads and upward motions of dark cavities, "bubbles" rising from the solar limb through the prominence. This prominence has a similar behavior as the prominence observed in Ca II H by Berger et al. (2008). The time-slice technique (Lin et al. 2005) allows us to determine quantitative values of the velocities $V(x, z)$ or V(trans) in the sky plane at different locations in the prominence observed by SOT. We adopt slices of 5 pixels (equivalent to 0.8″) with the east-west orientations (see Fig. 5, bottom). They follow nearly the common orientation as the fine structures of the prominence. The maximum angle between the east-west direction and the fine structures orientation is 30 degrees. For these structures, the measured velocities should be multiplied by a factor 1.25. We did not systematically apply this correction because for each thread, the angle is different. The high cadence of SOT (30 s) allows us to repeat the measurement of the velocities at each spatial point 5 times and determine the slope in the time slice diagram ($t = +/-1$ min). We estimate the accuracy of the measurements to be 1 km s^{-1}.

It appears that many structures in the time-slice diagrams (pixels close to each other along a slice) have the same velocity. A few of the threads exhibit different behaviors. These threads have in general higher velocities, reaching –10 km s^{-1} for a short time (5 to 10 min). The others commonly have a velocity of the order of –2 to –6 km s^{-1}. The trend is for downflows in the bright structures. The transverse velocity vector $V(x, z)$ and the norm of the velocity vector $|V| = \sqrt{[(V(y)^2 + V(x, z)^2)]}$ are indicated in Table 1 for these 12 points named in Fig. 5 (bottom). The letters used for SOT correspond to the location of the 12 points. According to the velocity vector, the fine structures are not really vertical but inclined from the vertical by an angle of between 30 degrees and 90 degrees. Some pixels exhibit upflows and later downflows. We identify these motions as stationary waves with periods of from ten to twenty minutes. If we were to assume that these pixels belong to vertical structures, the plasma would oscillate along or inside the structures; if the structures were horizontal, the structures themselves would oscillate like the transverse

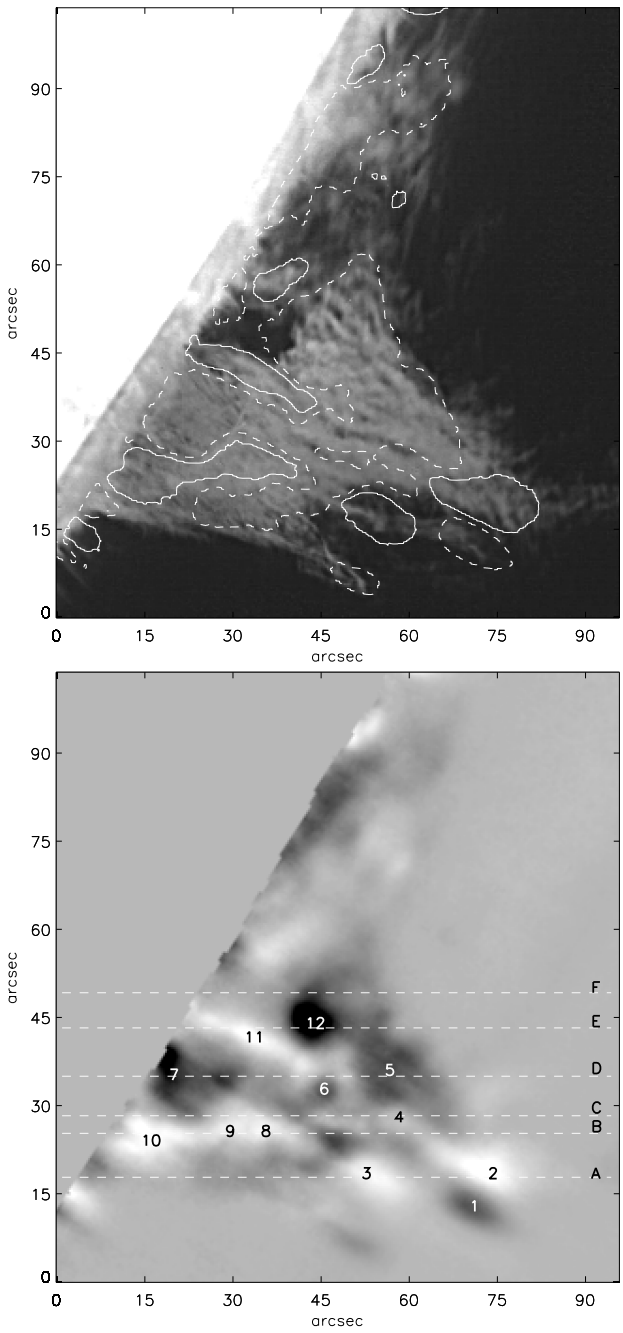

Fig. 5. *Top*: Hα *Hinode*/SOT image at 13:19 UT overlaid by Dopplershift contours, *bottom*: Dopplershift map of MSDP data at the same time. White/black areas (solid/dashed lines) correspond respectively to blue/redshifts. The dashed straight lines in the bottom image are the location of the slices used to compute the transverse velocity (A to F). The numbers are the points where Dopplershifts have been computed (see Table 1). Some profiles have been drawn in Fig. 6.

Table 1. MSDP Doppler shifts V (Doppler), velocity perpendicular to the line-of-sight V(trans), and norm of the velocity vector $|V|$ in 12 points of the prominence.

point MSDP	V(Doppler) km s^{-1}	V(trans) km s^{-1}	point SOT	$\|V\|$ km s^{-1}
1	+15	–	–	15
2	–5.5	–6	A2	8.5
3	–6.7	–2	A1	7
4	–0.6	+4	C	4
5	+1.8	–3	D2	3.5
6	+1.0	–2	D1	1.4
7	+3.0	–	–	3.0
8	−1.8	+3	B3	3.5
9	−1.8	+3	B2	3.5
10	−3.7	−2	B1	4.2
11	−3.6	+9	E1	9.7
12	+7.4	−11	E2	13.2

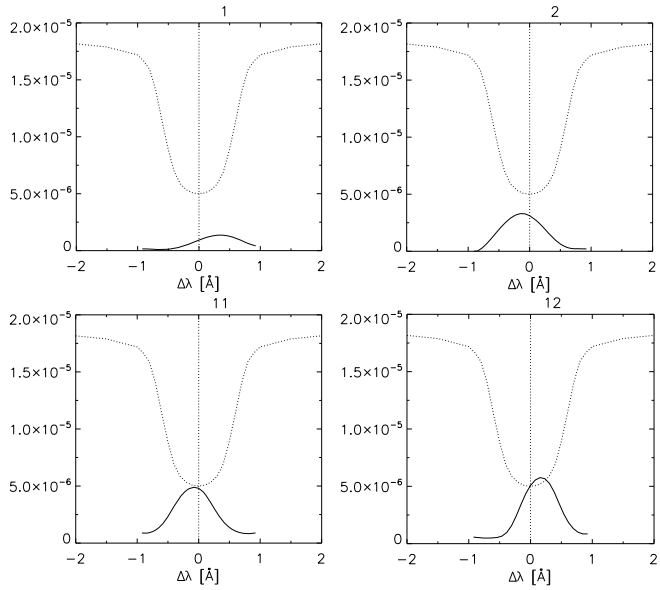

Fig. 6. Profiles of the Hα line in different points of the prominence observed with the MSDP at 13:19 UT (in erg/s/sr/cm^2/Hz). The numbers at the top of panels correspond to the points marked in Fig. 5. The intensities of profiles of the prominences (solid lines) have been multiplied by a factor 3 and compared with the reference line profiles observed on the disk. The scale in y-axis refers to reference profiles (dotted lines).

waves observed by Okamoto et al. (2007). Figure 7 shows the transverse velocities.

5. Discussion and conclusion

An Hα hedgerow prominence has been observed for the first time simultaneously with a high spatial resolution telescope (*Hinode*/SOT) and the spectrograph (MSDP) operating at the Meudon solar tower on April 25 2007. *Hinode*/SOT has allowed us to determine velocities perpendicular to the line-of-sight $V(x, z)$, and the MSDP, the velocity component along the line-of-sight $V(y)$ or Doppler-shifts. The prominence appears to have significant dynamics motion in the SOT movie with dark cavities rising from the limb with an upward velocity reaching 24 km s^{-1} and downflowing vertical-like bright threads. These threads move horizontally to avoid the dark cavities. During the rise of cavities, ahead of them, we observe bright curved fine structures from time to time with high velocities similar to the speed rise of the bubble. The *Hinode*/SOT observations have been calibrated by using the MSDP data. The integrated Hα intensity of the threads reaches 1.5×10^5 erg/s/sr/cm^2. The contrast in the dark cavities is between 70 and 90%.

The transverse velocities $V(x, z)$ of the bright threads are computed by using time-slice techniques and these values are of the order of beween a few km s^{-1} and 6 km s^{-1} reaching 11 km s^{-1} for individual fine threads. The pattern of the Doppler-shift map show elongated cells nearly perpendicular to

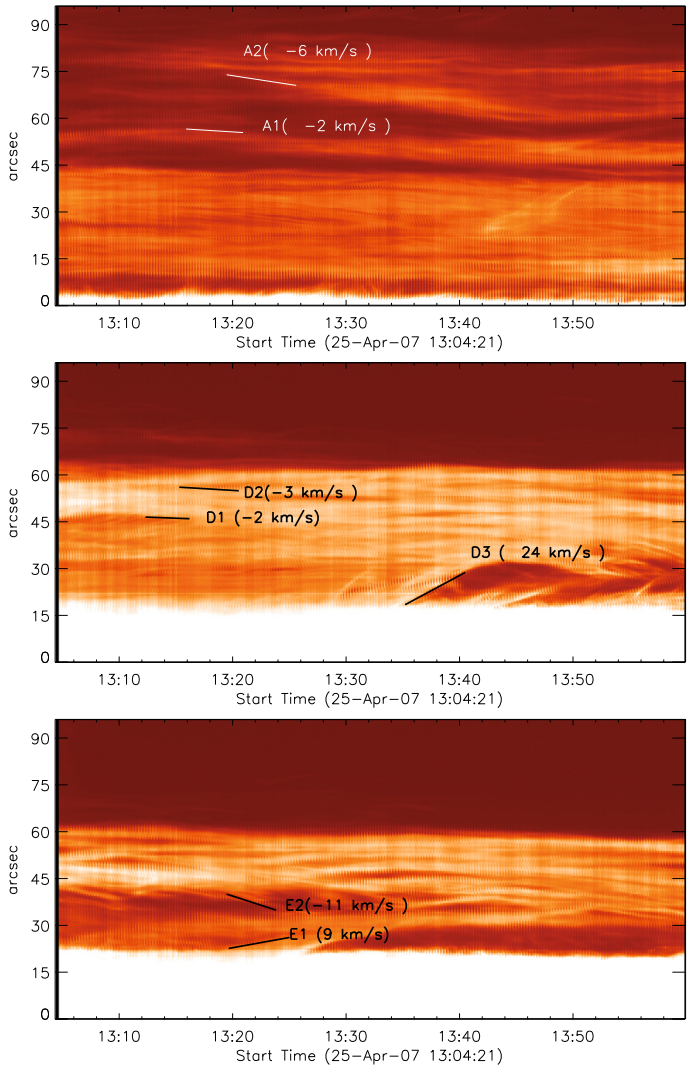

Fig. 7. Transverse velocities in SOT bright structures using time-slice technique (axis x unit is time, axis y unit is arcsec along the slide). Top/medium/bottom frame corresponds to slice A/ D/ E, respectively, drawn in Fig. 5. They show the velocities measured respectively at points A1, A2, D1, D2, E1, and E2 (Table 1). Positive/negative velocities correspond to up/down flows. The large value +24 km s^{-1} corresponds to the speed of a rising bubble from the limb or the flow speed of its bright edge. Fine threads close to the limb are spicules. Wave pattern corresponds to oscillations of period between 15 and 20 min. Adjacent pixels in a slice have coherent velocities.

the limb. They are wider than the MSDP spatial resolution. The time-slice maps contains several pixels close to each other along the slice that exhibit a similar velocity trend. This means that fine threads that are close to each other have coherent displacement. According to the observations of the prominence three days before when it remains on the disk as a filament, it appears that only the feet or barbs are dense enough to be observed. The prominence appears to represent the barb threads integrated along the line-of-sight as the filament crosses the limb. The structures are not vertical in the sky plane (x, z) as suggested by the movie. Doppler-shifts and transverse velocities are of similar orders of magnitude (smaller than 6 km s^{-1}), both measured with an estimated accuracy of 1 km s^{-1}. In Table 1, we have selected individual threads with the largest transverse velocities in regions of the highest Doppler shifts. The other parts of the prominence exhibit coherent velocities that are much smaller (1 to 2 km s^{-1}) and difficult to measure. The narrow Hα lines profiles of the prominence indicate that the different threads integrated along the line-of-sight have similar velocities. The dispersion in the velocities along the line-of-sight is small.

The longitudinal magnetic field observed (by the SOHO/MDI instrument) in the filament channel on the disk and at both edges of the inversion line is weak. The strength of the small polarities are weaker than 10 gauss. The prominence lies in a quiet region and corresponds to a quiescent filament. The small polarities can change rapidly and this might explain the fast dynamics of the structures.

In a flux tube model (Aulanier & Démoulin 1998a; Dudík et al. 2008), the Hα filament is considered to be cool material trapped in shallow dips along long magnetic field lines. The feet are extensions of the flux tube disturbed laterally by parasitic polarities. The barbs are piled-up dips touching the photosphere. When a parasitic polarity is canceled or moves, the feet move and can even disappear (Aulanier et al. 1998b; Schmieder et al. 2006; Gosain et al. 2009). In this 3D perspective, the prominence material should be trapped within inclined field lines and the downflow motion should occur along the shallow dips. The brightness would result from the integration of the threads along the line-of-sight (see Fig. 3e in Dudík et al. 2008). Aulanier et al. (1998b) explain very well by means of their magnetic extrapolation the relationship between parasitic polarities and the flux tube itself and their evolution. The flux of parasitic polarity should overcome that of the twisted flux tube and destroy the twisted configuration. The bubbles would be structures more magnetized than their surroundings and represented by the separatrices. A small increase in magnetic pressure in the bubble would lead to its rise inside the atmosphere. Strong currents can be created in the quasi separatrice layers (QSL) around the separatrices by photospheric displacements of the parasitic polarities (Démoulin et al. 1996). Energy release is expected. This could correspond to the brightening rims associated with filaments (Heinzel et al. 1995), which are not systematically visible because of the dense plasma of filaments. In SOT observations, the release may correspond to the bright top edge of the cavities where reconnection could occur and expel plasma. This would explain the high velocity material in brighter threads surrounding the dark cavities. During subsequent days, these bubbles are not observed in the prominence because the feet and parasitic polarities related to it should be on the back side of the disk. In the arcade model with dips proposed by Heinzel & Anzer (2001), the prominence observed on April 25 would consist of vertical threads trapped in dips and piled up giving the impression of vertical continuous threads. The downflows of 1 to 5 km s^{-1} would be caused by the shrinkage or successive reconnections of field lines.

Another explanation of the buoyancy of the dark cavities or bubbles could be adiabatic expansion of a heated volume of plasma (Berger et al. 2008). This is not exclusive of the magnetic pressure increase scenario and both magnetic and thermal buoyancy may play a role in the formation of these structures. We would like to measure the magnetic field in the bubbles and in the prominence. An other interesting study would be to analyse the EIS and SUMER data to see whether the dark bubbles are filled with hot material. These measurements are needed to determine which mechanism is valid for the formation of these dark low cavities.

Acknowledgements. We thank Nicolas Labrosse the chief planner of JOP 178 during the Hinode-SUMER campaign at MEDOC, operating center in Orsay who forecasted the correct pointing of this prominence three days in advance.

We thank T.E. Berger of the Lockheed Martin Solar and Astrophysic Laboratory for processing the *Hinode*/SOT data, for providing the movie, and for correcting the English language of the manuscript. R.C. thanks the CEFIPRA for his post-doctoral grant. This work in done in the frame of the European networks SOLAIRE and SOTERIA. We would like to thank the *Hinode* science team for the observations of SOT, the Meudon solar tower team for the MSDP observations particularly G. Molodij and J. Moity. We thank Guo Yang for his help in developing the time-slice procedure. The work of A.B. was supported by the Polish Ministry of Science and Higher Education (grant N203 016 32/2287), by the Academy of Sciences of the Czech Republic (grant M100030942) and the Observatoire de Paris. *Hinode* is a Japanese mission developed and launched by ISAS/JAXA, collaborating with NAOJ as a domestic partner, NASA and STFC (UK) as international partners.

References

Aulanier, G., & Démoulin, P. 1998a, A&A, 329, 1125
Aulanier, G., Démoulin, P., van Driel-Gesztelyi, L., Mein, P., & Deforest, C. 1998b, A&A, 335, 309
Berger, T. E., Shine, R. A., Slater, G. L., et al. 2008, ApJ, 676, L89
Chae, J., Ahn, K., Lim, E.-K., Choe, G. S., & Sakurai, T. 2008, ApJ, 689, L73
David, K.-H. 1961, Zeitschrift fur Astrophysik, 53, 37
d'Azambuja, L., & d'Azambuja, M. 1948, Ann. Obs. Paris-Meudon, 6, 7
Démoulin, P., Malherbe, J. M., & Priest, E. R. 1989, A&A, 211, 428
Démoulin, P., Hénoux, J. C., Priest, E. R., & Mandrini, C. H. 1996, A&A, 308, 643
Dudík, J., Aulanier, G., Schmieder, B., Bommier, V., & Roudier, T. 2008, Sol. Phys., 248, 29
Gosain, S., Schmieder, B., Venkatakrishnan, P., Chandra, R., & Artzner, G. 2009, Sol. Phys., 259, 13
Gouttebroze, P., Heinzel, P., & Vial, J. C. 1993, A&AS, 99, 513
Gunár, S., Heinzel, P., Schmieder, B., Schwartz, P., & Anzer, U. 2007, A&A, 472, 929
Heinzel, P., & Anzer, U. 2001, A&A, 375, 1082
Heinzel, P., Anzer, U., & Gunár, S. 2005, A&A, 442, 331
Heinzel, P., Kotrč, P., Mouradian, Z., & Buyukliev, G. T. 1995, Sol. Phys., 160, 19
Heinzel, P., Schmieder, B., Fárník, F., et al. 2008, ApJ, 686, 1383
Karpen, J. T., Antiochos, S. K., Klimchuk, J. A., & MacNeice, P. J. 2003, ApJ, 593, 1187
Karpen, J. T., Tanner, S. E. M., Antiochos, S. K., & DeVore, C. R. 2005, ApJ, 635, 1319
Kippenhahn, R., & Schlüter, A. 1957, Zeitschrift fur Astrophysik, 43, 36
Kosugi, T., Matsuzaki, K., Sakao, T., et al. 2007, Sol. Phys., 243, 3
Kuperus, M., & Raadu, M. A. 1974, A&A, 31, 189
Labrosse, N., Heinzel, P., & Vial, J. C. 2010, Space Sci. Rev., 151, 243
Lin, Y., Engvold, O., Rouppe van der Voort, L., Wiik, J. E., & Berger, T. E. 2005, Sol. Phys., 226, 239
Lin, Y., Engvold, O. R., & Wiik, J. E. 2003, Sol. Phys., 216, 109
Mackay, D. H., Karpen, J. T., Ballester, J. C., Schmieder, B., & Aulanier 2010, Space Sci. Rev., 151, 333
Malherbe, J. M. 1989, in Dynamics and Structure of Quiescent Solar Prominences, ed. E. R. Priest (Kluwer Academics Press.), 115
Mariska, J. T., & Poland, A. I. 1985, in BAAS, 17, 842
Mein, P. 1977, Sol. Phys., 54, 45
Mein, P. 1991, A&A, 248, 669
Mein, P., & Mein, N. 1991, Sol. Phys., 136, 317
Okamoto, T. J., Tsuneta, S., Berger, T. E., et al. 2007, Science, 318, 1577
Saito, K., & Tandberg-Hanssen, E. 1973, Sol. Phys., 31, 105
Schmieder, B. 1989, in Dynamics and Structure of Quiescent Solar Prominences, ed. E. R. Priest (Kluwer Academics Press.), 15
Schmieder, B., Aulanier, G., Mein, P., & López Ariste, A. 2006, Sol. Phys., 238, 245
Schmieder, B., Bommier, V., Kitai, R., et al. 2008, Sol. Phys., 247, 321
Schmieder, B., Raadu, M. A., & Wiik, J. E. 1991, A&A, 252, 353
Tandberg-Hanssen, E. 1994, in The nature of solar prominences (Kluwer Academics Press.), 113
Török, T., Aulanier, G., Schmieder, B., Reeves, K. K., & Golub, L. 2009, ApJ, 704, 485
van Ballegooijen, A. A., & Martens, P. C. H. 1989, ApJ, 343, 971
Zirker, J. B., Engvold, O., & Martin, S. F. 1998, Nature, 396, 440